Attributing urban evapotranspiration from eddy-covariance to surface cover: bottom-up versus top-down

H.J. Jongen[1,2], S. Vulova[3,4], F. Meier[5], G.J. Steeneveld[2], F.A. Jansen[1], D. Tetzlaff[6,7], B. Kleinschmit[3], N. Haacke[8]and A.J. Teuling[1]

[1]Hydrology and Environmental Hydraulics, Wageningen University, Wageningen, The Netherlands.
[2]Meteorology and Air Quality, Wageningen University, Wageningen, The Netherlands.
[3]Geoinformation in Environmental Planning Lab, Department of Landscape Architecture and Environmental Planning, Technische Universität Berlin, Berlin, Germany
[4]Department of Environmental Meteorology, Institute for Landscape Architecture and Landscape Planning, University of Kassel, Kassel, Germany
[5]Chair of Climatology, Technische Universität Berlin, Berlin, Germany.
[6]Department of Ecohydrology, Leibniz Institute of Freshwater Ecology and Inland Fisheries, Berlin, Germany.
[7]Department of Geography, Humboldt University of Berlin, Berlin, Germany.
[8]Ecohydrology and Landscape Evaluation, Institute of Ecology, Technical University Berlin, Berlin, Germany.

Key Points:

- Urban eddy-covariance footprints distinctly differ in surface cover composition from hour to hour.
- Impervious surfaces evaporate less than their surface fraction, but their contribution cannot be neglected.
- High vegetation contributes up to 50% more to the total evaporation than its surface fraction in this study.

Corresponding author: Harro Jongen, `harro.jongen@wur.nl`

Abstract

Evapotranspiration (ET) is a key process in the hydrological cycle that can help mitigate urban heat. ET depends on the surface cover, as the surface affects the partitioning of precipitation between runoff and evapotranspiration. In urban neighborhoods, this surface cover is highly heterogeneous. The resulting neighborhood-scale ET is observed with eddy-covariance systems. However, these observations represent the signal from wind- and stability-dependent footprints resulting in a continuously changing surface cover composition. This continuous change prevents quantitative analysis of the separate types. Here, we disentangle this neighborhood-scale ET at two urban sites in Berlin attributing the ET dynamics to the four major surface cover types in the footprint: impervious surfaces, low vegetation, high vegetation, and open water. Starting from the surface, we reconstruct ET based on patch-scale observations and conceptual models. Alternatively, we start with the eddy-covariance observations and attribute ET to the surface cover types solving a system of equations for four eddy-covariance systems with different footprints. Although starting at the surface yields more robust results, both approaches indicate that vegetation is responsible for more ET than proportional to its surface fraction, and evaporation from impervious surfaces although less cannot be neglected. We confirm the intuitive relation between ET and the surface cover fractions based on a wide range of surface compositions.

Plain Language Summary

Different types of surfaces, like grass, trees, pavement, and open water, affect how rainwater is divided between evaporation and runoff. In cities with lots of pavement and buildings, more water runs off than in natural areas leaving less water for evaporation. Measurement towers have been observing the evaporation from whole neighborhoods, but separating the effects of different surfaces is hard. In our study, we figure out how much each surface type contributes to evaporation with two methods: one starting from the separate surfaces and rebuilding the neighborhood evaporation, and the other starting with the neighborhood evaporation and breaking it down into evaporation from each surface. Both ways showed that plants evaporate more than proportionally to their surface area, but even built surfaces like pavement evaporate. Our findings confirm that more plants lead to more evaporation, but built surfaces cannot be ignored. This information can help urban planners create cities that manage water better, making cities nicer places to live.

1 Introduction

How precipitation is partitioned between runoff and evapotranspiration (ET) plays an important role in the urban climate and is governed by the surface cover composition (Paul & Meyer, 2001; Oke et al., 2017). In cities, the abundant impervious surfaces prevent infiltration and promote surface runoff leaving less water available for ET than pervious areas (Fletcher et al., 2013; McGrane, 2016; Jongen et al., 2022). On the other hand, urban vegetation has the opposite effect increasing infiltration and ET (Peters et al., 2011; Gunawardena et al., 2017). While all vegetation favors ET compared to impervious surfaces, an isotope-based study revealed the vegetation type also affects infiltration and ET patterns (Kuhlemann et al., 2021). The combination of surface covers thus controls the water partitioning and consequently ET dynamics.

Promoting green surface covers by planting vegetation can increase ET using more of the available energy (Wang & Shu, 2020). Like vegetation, open water is suggested to potentially cool its surroundings by evaporation when implemented appropriately (Solcerova et al., 2019; Jacobs et al., 2020), although warming can also occur due to the high thermal inertia (Theeuwes et al., 2013; Steeneveld et al., 2014). The energy needed for the additional ET cannot heat the air mitigating heat and the associated health risks (Oke, 1982; Heaviside et al., 2017; Ward & Grimmond, 2017). However, how surface cover composition at the patch level ($\sim 10^1 - 10^2$ m of a single surface cover type) translates to the neighborhood scale ($\sim 10^3$ m) is largely unknown until now. To answer this question, we need to quantify how surface cover impacts the partitioning of incoming water fluxes (Bonneau et al., 2018) and how this affects the partitioning on the larger, neighborhood scale. Ultimately, the neighborhood scale is where the effect of the surface covers on ET needs to be understood. In time, this understanding will support the management of the cooling benefits and urban water demands.

At the neighborhood scale, eddy-covariance (EC) systems observe the ET of the combined surface cover types in their footprint (Feigenwinter et al., 2012). We refer to this as ET, since these observations show the combined signal of contributions from the present surface cover types and thus include evaporation, transpiration, and anthropogenic fluxes. Even though the heterogeneous urban surface results in spatially variable ET (Qin et al., 2022), the observed ET represents the weighted average flux in the footprint, as the EC systems are typically installed at a height where the heterogeneous surface flux sources are blended (Oke et al., 2017). Apart from this height, the footprint varies temporally depending on the wind speed and direction, and atmospheric stability (Kljun et al., 2015). Previous research demonstrated it is possible to upscale patch-scale ET observations to the neighborhood-scale EC observations weighed by surface cover in the footprint climatology at a relatively homogeneous urban site (Peters et al., 2011). However, hour-to-hour variation in the footprint contains useful information to understand ET. This time-dependent surface information has been applied to improve the model performance of urban ET machine learning models (Vulova et al., 2021). Thus, for the more common heterogeneous urban sites, the footprint is crucial information to disentangle the neighborhood-scale ET and attribute it to the different surface cover types.

EC footprints can be estimated with a variety of models. Large-eddy simulations (LES) or Lagrangian stochastic particle dispersion models (LPD) fully model the airflow to find the source area (LES: Leclerc et al. (1997); Wang and Davis (2008); LPD: Kljun et al. (2002); Hsieh et al. (2003); LES and LPD combined: Hellsten et al. (2015); Auvinen et al. (2017)). These models are both labor-intensive and computationally expensive, which limits their applicability to relatively short case studies (Vesala et al., 2008). To analyze longer time series, faster footprint models have been developed with an analytical approach relying on the surface-layer theory (e.g. Schuepp et al., 1990; Schmid & Oke, 1990; Kormann & Meixner, 2001). Their validity is restricted to certain turbulence intensities or stratifications. More recently, Kljun et al. (2015) developed a two-dimensional footprint parameterization that takes away these limitations. Their model yields robust results for most boundary layer conditions at any observation height within the surface layer. This model enables the identification of the flux's source area for a long time series with a wide range of atmospheric conditions. Therefore, this model is suitable to study the influence of the changing footprints on ET.

To study the influence of surface cover on ET, Peters et al. (2011) have described the seasonal patterns in urban ET from major plant-functional types (trees and turf grass). These two vegetation types explain the majority of ET variation. They also find that the surface fraction of a vegetation type is the most important factor determining its contribution to total ET underlining the importance of the EC footprint. They assume impervious surface evaporation can be neglected, while other studies show this assumption may not be valid (Ramamurthy & Bou-Zeid, 2014; Chen et al., 2023). Below, we will test the assumption by including evaporation from impervious surfaces. Moreover, while their analysis is focused on the seasonal timescale, we will consider the hourly timescale. The hourly ET dynamics play a key role in the urban climate experienced by urban citizens. As a verification, Peters et al. (2011) compared the sum of their ET components against EC observations, in essence reconstructing the ET signal from the bottom up.

Very few cities have observations of all relevant hydrometeorological states and fluxes across a range of surface covers. Berlin is a notable exception. In Berlin, meteorological observations are performed as part of two observatories: the Urban Climate Observatory operated by the Chair of Climatology at the Technische Universität Berlin (https://uco.berlin/en, Scherer et al., 2019) and the Steglitz Urban Ecohydrological Observatory from the IGB Leibniz-Institute of Freshwater Ecology and Inland Fisheries (Kuhlemann et al., 2020, 2021). Additionally, campaigns have added to this observation infrastructure, for example, with drone-based observations (Vulova et al., 2019) or with ground-based remote sensing (Zeeman et al., 2023). The elaborate observation infrastructure has resulted in numerous studies focusing on Berlin (e.g. Meier & Scherer, 2012; Fenner et al., 2014, 2023), of which many focused on ET. Kuhlemann et al. (2021) show based on soil isotopes that ET differs depending on the vegetation type with more interception but less soil evaporation for higher vegetation types. Subsequently, these isotope observations provide the means to evaluate modeled water partitioning quantifying yearly ET fluxes for different vegetation types (Gillefalk et al., 2021, 2022). Another modeling study applied a physics-based model to study hourly ET (Duarte Rocha et al., 2022), which after validation was combined with remotely-sensed vegetation characteristics to map ET for all of Berlin (Rocha et al., 2022). Vulova et al. (2021) achieved similar modeling skill with machine learning trained on meteorological and remote sensing data. Because of the research infrastructure and the extensive literature, Berlin offers a unique setting to study the link between the surface cover and ET.

While the evaporation dynamics from various surface cover types have been investigated previously, few studies have addressed these issues across a range of surface cover types. These studies show that surface cover types have very different evaporation dynamics. Four main surface cover types can be distinguished: impervious surface, low vegetation, high vegetation, and open water. Impervious surfaces only evaporate when wet directly after rainfall resulting in highly dynamic evaporation (Wouters et al., 2015). In contrast, vegetation can draw water from the soil sustaining ET long after rainfall (Teuling et al., 2006; Boese et al., 2019). Amongst vegetation, differences are seen with higher average ET for higher vegetation with its higher leaf area density than for lower vegetation (Gillefalk et al., 2021). Sufficiently deep open water has more constant evaporation given the abundant water and high heat storage capacity that can provide energy in the absence of solar radiation (Jansen et al., 2022). The term ET is used for vegetation because the combined signal from transpiration, interception, and soil evaporation is considered. Over impervious and open water surfaces, only evaporation occurs so the term evaporation is used. We hypothesize these behaviors are combined at the neighborhood scale, as observed with EC, dependent on their relative contribution to the surface.

In this study, we aim to estimate the ET contribution of different surface cover types in the footprint profiting from the diverse observations in Berlin. With this, we will show how the footprint varies over time, how ET behaves for each surface cover type, the relation between the surface cover and neighborhood ET, and the contribution of each surface cover type to neighborhood ET. To study the contribution of each surface cover type to ET, we take both a bottom-up and a top-down approach to attribute the EC-observed ET to the four dominant surface cover types. For the bottom-up approach, we reconstruct the EC signal by summing the estimated ET contribution of each surface cover type weighed by its contribution to the footprint. In this approach, the ET contribution of each type is mimicked with conceptual models and small-scale observations. The top-down approach is based on a system of equations, in which each equation describes the surface cover composition of one EC system and its resulting flux. The resulting flux can be attributed to the surface cover types by solving the system of equations. We aim to reveal how the surface cover type influences neighborhood ET behavior and to indicate how altering surface cover may affect urban climate. Understanding the relationship between urban surface cover and ET can inform future climate-resilient urban design.

2 Study sites

This study examines observations from the capital and largest city of Germany, Berlin, which has a population of 3.7 million spread over 891 km^2 (Amt für Statistik Berlin-Brandenburg, 2019). Situated in the east of Germany, the climate is temperate oceanic (Cfb) (Kottek et al., 2006). The closest weather station from the German Weather Service (DWD, Berlin-Tempelhof) recorded a long-term (1991-2020) mean annual rainfall of 585 mm and mean air temperature of 10.2 °C (DWD, 2021b). Here, we study the warm months (April until October) of the relatively dry year of 2019 with 492 mm of precipitation, in which an intense observation campaign was organized (Vulova et al., 2019). The warm months are studied as most ET occurs during this time.

Two sites in Berlin are studied here: a suburban one and one close to the city center. The first, suburban site is an urban research garden located in the southwest of the city at the Rothenburgstraße (ROTH, 52.457°N, 13.315°E, Figure 1a, (Vulova et al., 2021)). This site is an ICOS (Integrated Carbon Observation System) Associated Ecosystem Station (DE-BeR). Its surroundings within 1 km consist of 47% impervious surface, 19% low vegetation, 34% high vegetation, and no open water (see Sec. 3.1). At ROTH, a 40-meter tower holds three EC systems (IRGASON, Campbell Scientific) at 2, 30, and 40 meters. For all EC systems in this study, the resolution is 30 minutes. The observations are quality controlled according to the literature and only high-quality data (flag 0) is used (Foken et al., 2004). Additionally, sap flow was observed at six trees with FLGS-TDP XM1000 sap velocity logger systems (Dynamax Inc, Houston, USA), and soil moisture content was measured in two locations below high vegetation at three depths: 10-15, 40-50, and 90-100 cm (CS650 reflectometers, Campbell Scientific) (Kuhlemann et al., 2020). Finally, the leaf area index was measured monthly over three transects through high vegetation (LAI-2200, LI-COR, Lincoln, USA) (Vulova et al., 2019). Along each transect, leaf area index measurements were conducted at 1-meter intervals to capture the canopy variability, while walking in the same direction each time for standardization. A tripod on a balcony served as a reference for the above-canopy light conditions measuring every 10 seconds.

The second site is close to the city center at the TU Berlin Campus Charlottenburg (TUCC, 52.512°N, 13.328°E, Figure 1b, (Vulova et al., 2019; Jin et al., 2021)). Its surroundings within 1 km are more impervious than at ROTH: 62% impervious surface, 8% low vegetation, 26% high vegetation, and 3% open water (see Sec. 3.1). On the roof of TU Berlin (building height 46 meters), observations are made with a ceilometer (Lufft CHM 15k) and an EC system (IRGASON, Campbell Scientific). The EC system is attached to a 10-meter tower reaching 56 meters above ground level.

3 Methods

3.1 Surface cover classification

The surface cover needs to be classified to link the surface in the EC footprint to the neighborhood-scale ET observed with the EC system. Given the surface fraction covered by each surface cover type, the ET can be reconstructed from the evaporation dynamics of the different surface cover types (bottom-up, Figure 2a) or attributed to the surface cover types by linear decomposition (top-down, Figure 2b). For this study, we classify the surface into four different surface cover types: impervious surface, low vegetation, high vegetation, and open water. For this purpose, we combine information from four geospatial datasets from Berlin Open Data and the Berlin Digital Environmental Atlas:

- *Building height*: raster dataset at a 1-meter spatial resolution of all buildings in Berlin (Senate Department for Urban Development, Building and Housing, 2012).

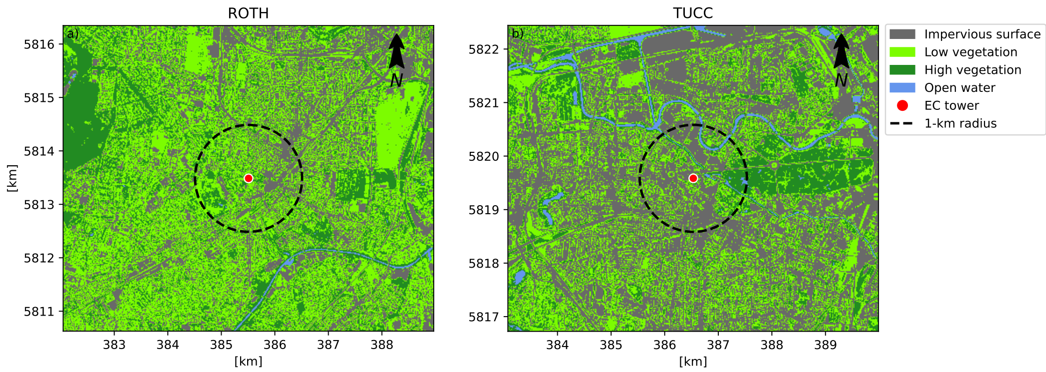

Figure 1. Map of Berlin indicating the location of the (a) ROTH and (b) TUCC study sites with their surroundings classified in the four surface cover types distinguished in this study with the 1-km radius (dashed black line) around the EC towers (red dots). The coordinate reference system is WGS 84 UTM/33N EPSG: 32633)

- *Vegetation height*: raster dataset at a 1-meter spatial resolution of all vegetation including trees, bushes, and grass in Berlin (Senate Department for Urban Development, Building and Housing, 2012)
- *Biotope types*: vector dataset describing the biotope type of all vegetation in Berlin according to the 7483 biotope types described by Zimmermann et al. (2015) (Senate Department for Urban Development, Building and Housing, 2013)
- *Streets*: vector dataset with all road segments in Berlin (Senate Department for the Environment, Mobility, Consumer and Climate Protection Berlin, 2014)

Around each EC tower, we classified the surface covers with a buffer of 0.025 degrees latitude and 0.05 degrees longitude in both directions, equivalent to 2.8 and 3.4 kilometers. In total, this gives an area of 5.6 by 6.8 kilometers. We selected this buffer, as for 90% of the footprints this area includes the entire footprint calculated in this study (see Sec. 3.2). For only 0.5% of the time, the buffer contains less than 80% of the footprint. All datasets are clipped to this area. Vector datasets are resampled to rasters at a 1-meter resolution to ensure compatibility with the raster datasets.

At the start of the classification, all described vegetated land biotopes are assigned to vegetation and all water biotopes to open water. The impervious surface is determined based on all areas in the street data and all areas that have an assigned building height. The vegetation is split into low and high vegetation depending on the height with a threshold of 0.5 meters following Kuhlemann et al. (2021). The exact threshold has minimal influence as only a negligible fraction of the vegetation has a height between 0.3 and 1.0 meters.

3.2 Footprint modeling

Footprints were calculated to determine the source area of the turbulent fluxes for all timesteps. We selected the flux footprint model from Kljun et al. (2015), which is frequently applied in urban environments (e.g. Stagakis et al., 2019; Nicolini et al., 2022; Karl et al., 2023). This footprint model provides two-dimensional grids with relative flux contribution. The model requires the measurement height, friction velocity, boundary-layer height, Obukhov length, wind direction, and mean and standard deviation of the wind speed. For all wind variables, EC observations are used, while the boundary-layer height is derived from ceilometer observations at the TUCC site. The Obukhov length

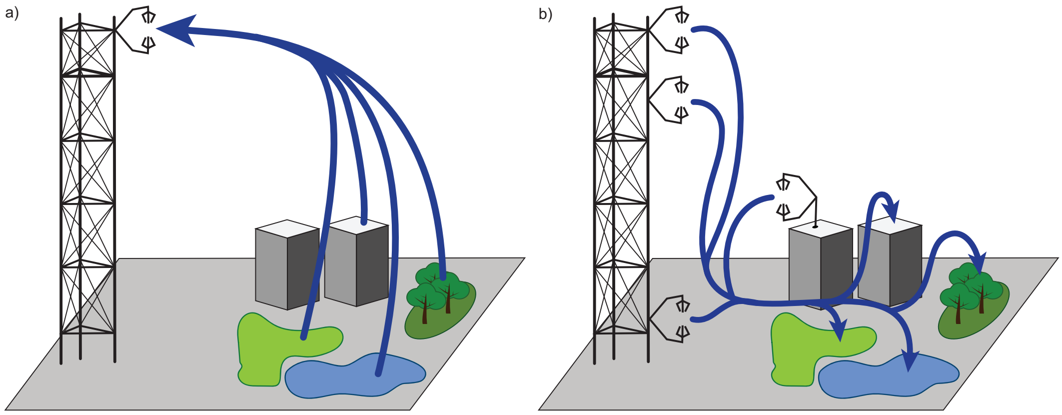

Figure 2. Conceptual drawing of the bottom-up (a) and top-down (b) approach. The arrows start at the data sources and end at the results of the approaches. Footprints determine the contribution for each surface cover type (not shown).

in m (L) is calculated according to:

$$L = -\frac{u_*^3 \bar{\theta}_v}{\kappa g (\overline{w'\theta_v'})_s} \tag{1}$$

where u_* the surface friction velocity in m s^{-1}, $\bar{\theta}_v$ the mean virtual potential temperature in K, κ the von Kármán constant of 0.4, g the gravitational acceleration of 9.81 m s^{-2}, and $(\overline{w'\theta_v'})_s$ the kinematic virtual potential temperature flux in K m s^{-1} at the observation height.

As the model results in contours per 10% and the 100%-contribution contour is infinite, the resulting footprint grids are limited to the 90%-contribution contour. Part of the footprint is not taken into account when the footprint extends beyond the classified area (Section 3.1). This last step had minimal influence, as the classified area is considerably larger than the typically considered representative area within a radius of either 0.5 or 1 kilometer (Lipson et al., 2022). In the end, the surface fractions are calculated as the footprint contribution per surface cover type taking into account the weight of each pixel.

3.3 Bottom-up

The bottom-up approach attributes ET to the different surface cover types by determining evaporation dynamics for each type (Figure 2a). Consequently, the EC observations are hypothesized to be reconstructed when these dynamics are weighed with the footprint contribution of the surface cover types. For the impervious surfaces, open water, and high vegetation interception, evaporation dynamics are estimated based on conceptual models. For the low vegetation and the high vegetation transpiration, observations capture the dynamics. We assume the evaporation dynamics per surface cover type to be similar for ROTH and TUCC, as previous research found their forcing is comparable and can be used interchangeably to predict ET with the same accuracy (Duarte Rocha et al., 2022). Negative ET observations are omitted, as the conceptual models are not capable of predicting negative fluxes. This filter has a very limited impact on the results, as it excludes only 384 of the 17780 30-minute time intervals. The results are analyzed at two timescales, midday and daily, as these consider different aspects of ET. Midday is defined from 11:00 until 15:00 local (10:00-14:00 UTC) time with every half hour considered separately. During these hours, incoming radiation driving ET is highest. Considering multiple hours minimizes the sampling noise due to the stochastic nature of turbulence even at half-hourly timescales. The daily timescale is relevant for water resources management.

Impervious surface

Evaporation from impervious surfaces is modeled according to Wouters et al. (2015). Their parameterization includes two processes to mimic the water on an impervious surface: rainfall and evaporation. The impervious surface is characterized by the maximum water storage (w_m) in mm m^{-2} and the maximum wet/evaporative fraction (δ_m). These parameters were determined for Berlin based on 3D-LIDAR scans and found to be 1.03 mm m^{-2} and 13.53% (Haacke, 2022). The evaporative fraction decreases following a power law with an exponent of $-\frac{2}{3}$ depending on the water storage, which follows from the assumption that interception storage capacity linearly depends on the storage depth. Water gain from rainfall is reduced in efficiency when closer to the water storage described by:

$$w(t+\Delta t) = w_m \left(1 - \ln(1 - (1 - e^{(1-\frac{w(t)}{w_m})})e^{-\frac{r_0 \Delta t}{w_m}})\right) \quad (2)$$

where, w is the water storage in mm, t time in s, Δt length of the time step in s, and r_0 the rainfall intensity in mm s^{-1}. The formulation assumes constant rainfall during a time step. The evaporation is described by:

$$w(t+\Delta t) = \left(w(t)^{\frac{1}{3}} - \frac{\delta_m E_p \Delta t}{3w_m^{\frac{2}{3}}}\right)^3 \quad (3)$$

where E_p is the potential evaporation. The E_p is calculated according to Penman (1956), further described in Eq. 4. The meteorological forcing has a resolution of 30 minutes, but the conceptual model is run numerically at a 30-second time step to ensure a numerically robust solution with linearly interpolated meteorological forcing.

High vegetation

The ET from high vegetation consists of transpiration and interception. The transpiration is derived from observations of the soil moisture content and sap flow as described in Kuhlemann et al. (2021). Soil moisture content observations are used from both the “Trees” and “Shrubs” plots for the transpiration estimation from high vegetation. The soil moisture content reflects the evaporated water volume, but root water uptake does not correlate directly with transpiration apparent from the lag between the two. Therefore, we scale daily soil moisture loss with hourly sap flow observations. This method takes advantage of the temporal variation in sap flow observations and the magnitude of the soil moisture content observations. Soil moisture loss due to drainage is assumed to be negligible, as the deepest soil moisture observations at 95 cm depth do not indicate a drainage flux. Furthermore, soil moisture loss in the lowest layer of observations is not added to the evaporation.

The canopy interception and its evaporation are modeled with the Rutter model that allows for sub-daily resolution (Rutter et al., 1975; Valente et al., 1997). The model partitions rainfall between evaporation from the canopy and trunk, throughfall, and stem flow. Two storages are part of the model: the canopy and the trunk. Both storages evaporate at the potential rate calculated according to the Penman (1956) equation (Eq. 4). Canopy storage capacity depends on the tree species ranging between 0.1 and 3 mm (e.g. Aston, 1979; Klaassen et al., 1998; Baptista et al., 2018; Ramírez et al., 2018), although in exceptional tropical canopies capacities up to 8 mm have been observed (Herwitz, 1985). We assume the canopy storage capacity is linearly related to the leaf area index with a storage of 0.2 mm per unit leaf area (Huang et al., 2017). Leaf area index observations at monthly intervals are interpolated with a univariate spline with four degrees of freedom. The modeled interception appears to be relatively insensitive to the other parameters: trunk water storage capacity, partitioning between stem flow and throughfall, and the fraction of evaporation from the stem flow. All of these parameters concern the stem flow, which, on average, accounts for only 2% of the precipitation exceeding the canopy storage capacity (Rutter et al., 1975). The modeled interception evaporation is added to the transpiration to obtain the ET from the high vegetation.

Low vegetation

Low vegetation is directly represented by an EC system installed at 2 meters directly above the grass at ROTH. In their similar study, Peters et al. (2011) installed an EC system close to the surface to estimate the ET from low vegetation as well. Within a forest, a comparable set-up helped to differentiate the ET components (Paul-Limoges et al., 2020).

The quality-controlled ET is a direct observation of the low vegetation dynamics when the wind comes from between east (90°) and southwest (230°). Fluxes were only considered when suitable for process-focused studies (quality flag "0" according to Foken et al. (2004)).

Open water

Open water evaporation is estimated with a parameterization of the Penman (1956) equation (De Bruin, 1979):

$$E_p = 37 + 40\overline{u}_{2m}(e_{s,2m} - e_{40m}) \tag{4}$$

where $\overline{u}_{2m}$ is the mean wind speed at 2 meters (m s^{-1}), $e_{s,2m}$ the saturated vapor pressure at 2 meters (Pa), and e_{40m} the vapor pressure at 40 meters (Pa). Open water is assumed to evaporate at the potential rate. In the case of a negative E_p, evaporation is set to 0.

3.4 Top-down

The top-down approach takes the neighborhood-scale EC observations and attributes the flux to the different surface cover types by solving a system of equations (Figure 2b). The system consists of four equations. Each equation describes how the surface covers are combined according to the footprint to yield the EC observation. The evaporation for the four surface cover types results in four unknowns, as the evaporation per surface cover type is assumed similar for all EC systems. The linear system can be solved, as it has an equal number of equations and unknowns.

$$f_{im,1}E_{im} + f_{lv,1}E_{lv} + f_{hv,1}E_{hv} + f_{ow,1}E_{ow} = E_{EC,1} \tag{5}$$

$$f_{im,2}E_{im} + f_{lv,2}E_{lv} + f_{hv,2}E_{hv} + f_{ow,2}E_{ow} = E_{EC,2} \tag{6}$$

$$f_{im,3}E_{im} + f_{lv,3}E_{lv} + f_{hv,3}E_{hv} + f_{ow,3}E_{ow} = E_{EC,3} \tag{7}$$

$$f_{im,4}E_{im} + f_{lv,4}E_{lv} + f_{hv,4}E_{hv} + f_{ow,4}E_{ow} = E_{EC,4} \tag{8}$$

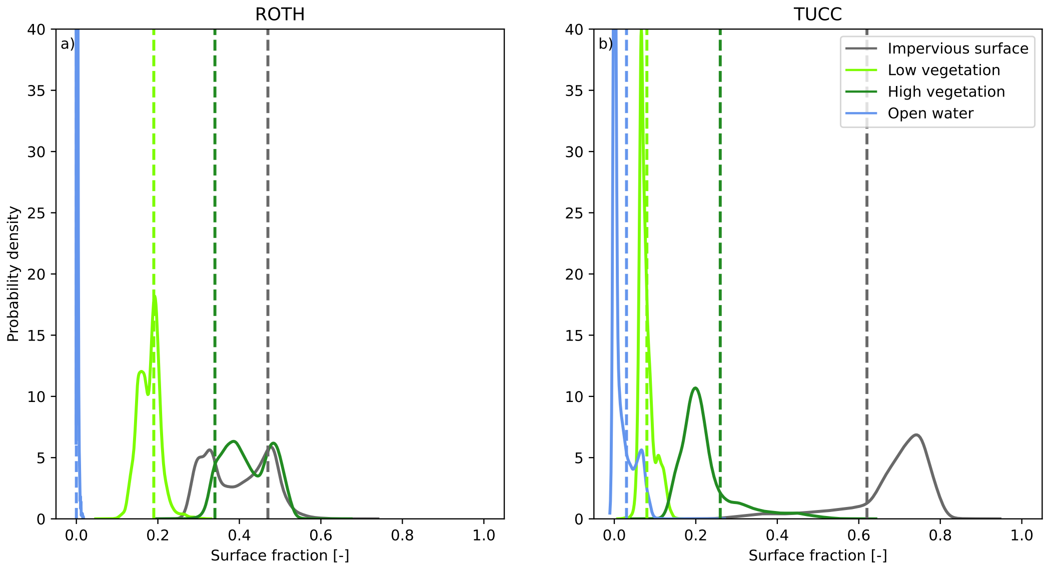

Figure 3. Probability density of the time-dependent surface fractions in the EC footprint over the study period (April-October 2019). The dashed vertical lines indicate the average surface cover fraction within a 1-km radius of the EC (see Figure 1).

where f is the fraction of the impervious surface (im), low vegetation (lv), high vegetation (hv), and open water (ow), and E is evaporation of the same surfaces and the EC. The numbers indicate the different EC systems. The four EC systems are at the 56-m EC at TUCC and 2-, 30-, and 40-m ECs at ROTH. The evaporation from each surface can be determined given the fractions derived from the footprints and the EC observations. We exclude solutions with estimated evaporation below -3.5 mm d^{-1} for one of the surface cover types, as these solutions likely have negative evaporation rates for one surface cover type that are balanced by positive evaporation rates for another type.

4 Results

4.1 Footprint variation

A high variation in footprint composition highlights the heterogeneity of the urban surface (Figure 3). The wide, non-normal distributions cause the actual surface fractions in the footprint to differ substantially from the surface cover fractions within a 1-km radius of the EC system (vertical lines) at most times. The 1-km radius estimation and the actual fraction are only similar for open water, as this covers a limited surface. For the impervious surface and high vegetation at ROTH, the bi-modality of the distribution demonstrates that a single value will not be able to capture the surface fractions. Additionally, surface covers can vary within a wide range as seen at TUCC where the impervious surface fraction varies from 0.2 up to 0.8. The high variation necessitates that the time-dependent footprint composition is considered to understand ET dynamics.

4.2 Surface cover composition impact on evapotranspiration

Combining the footprint variation from both sites with the neighborhood ET reveals the influence of the surface cover composition on ET (Figure 4). We find less ET with more impervious surface and more ET with more vegetation (high and low). Open water shows a less clear relation, as the open water fraction is very low most of the time.

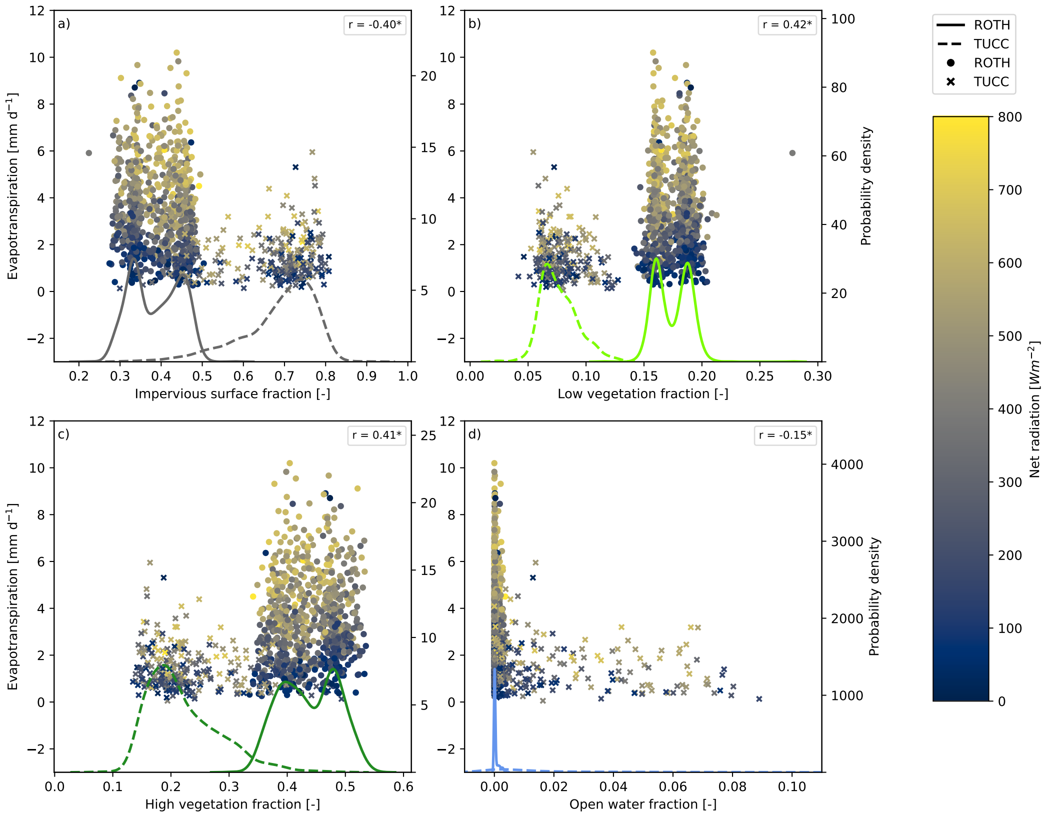

Figure 4. Relation of the observed ET and the surface cover fraction for each surface cover type (a: impervious surface, b: low vegetation, c: high vegetation, d: open water). The probability density curves (right axis) describe the footprint compositions for both ROTH (solid) and TUCC (dashed).

Although the surface cover is relevant, the variation in the ET indicates meteorological conditions affect ET as well, illustrated by the ordering of the points by available energy quantified as the net radiation. While the surface cover composition in the footprint varies at one site, the two sites together reveal an evident influence of the surface on ET.

4.3 Evapotranspiration attribution to the surface cover

Observed ET is approximated by ET reconstructed by a weighted average of surface cover type evaporation dynamics (Figure 5 and Table 1). Performance depends on surface cover, as results show consistently higher correlations at ROTH compared to the more impervious TUCC. Additionally, the negative MBE indicates an underestimation of total ET. The data gaps due to quality control of the 2-m EC system explain why the number of evaluated data points is lower than the duration of the study period. In two TUCC cases, ET is highly overestimated when a rainfall event coincides with a high impervious fraction in the footprint and high potential evaporation (Figure 5c), for which the conceptual model for impervious surfaces is responsible.

Absolute errors increase with rising ET rates across both timescales at ROTH (Figure 5). Other than with ET itself, the absolute errors correlate with the meteorological and hydrological conditions (Table 2). The observed net radiation has a positive correlation with the absolute ET error at ROTH while no correlation is present at TUCC.

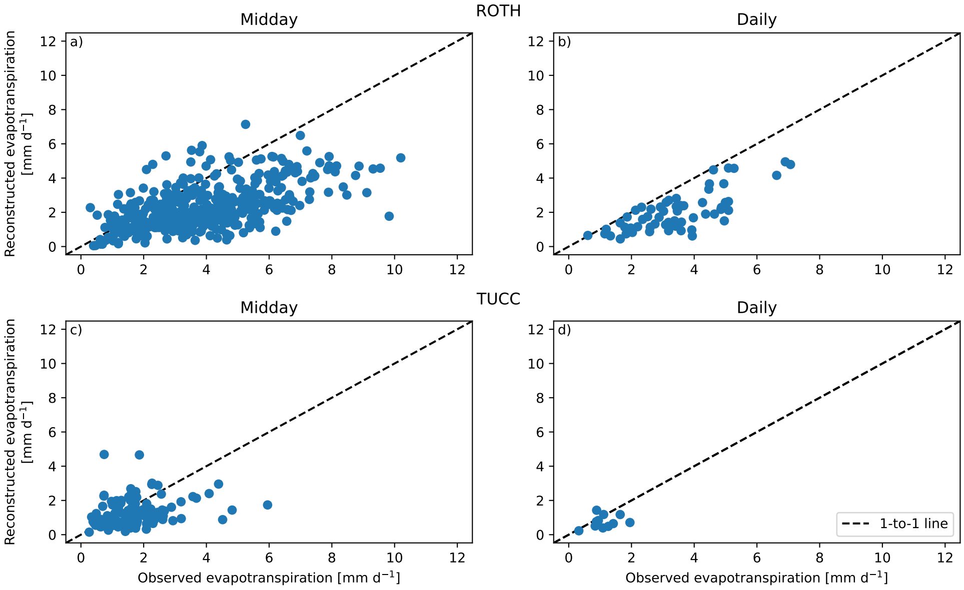

Figure 5. Comparison of the *ET* observed with EC against the *ET* reconstructed with small-scale observations and conceptual models at (a-b) Rothenburgstraße and (c-d) TU Berlin campus for (a,c) midday hours per half hour and (b,d) daily means. Midday hours are between 11:00 and 15:00 local time (10:00-14:00 UTC). Table 1 gives an overview of the statistics.

Table 1. Overview of the performance of the bottom-up approach compared with EC *ET* observations per 30 minutes as shown in Figure 5.

		Rothenburgstraße		**TU Berlin campus**	
		Midday	*Daily*	*Midday*	*Daily*
Figure 5	panel	a	b	c	d
Data points	[-]	440	60	113	11
Observed mean *ET*	[mm d^{-1}]	3.9	3.4	1.7	1.1
Modeled mean *ET*	[mm d^{-1}]	2.3	2.0	1.3	0.8
Mean bias error	[mm d^{-1}]	-1.6	-1.4	-0.4	-0.4
Mean absolute error	[mm d^{-1}]	1.8	1.4	0.9	0.5
Pearson's r	[-]	0.56	0.76	0.29	0.27

Table 2. Overview of Pearson correlations between environmental variables and the absolute error of the bottom-up reconstructed ET. Only significant correlations are shown (Wald's test).

	Rothenburgstraße		**TU Berlin campus**	
	Midday	*Days*	*Midday*	*Days*
Net radiation	0.39	0.18		
Soil moisture	-0.34			
Specific humidity	0.35	0.20	0.16	
Vapour pressure deficit	0.45			
Impervious evaporation			0.59	0.86

This suggests the bottom-up approach performs worse with more available energy. At the same time, soil moisture values show a negative correlation at ROTH suggesting errors are smaller for relatively wet soil conditions. At TUCC, soil moisture does not correlate with the error, which could be explained by the high impervious fraction. The specific humidity shows errors increase with more moist air. In contrast, vapor pressure deficit indicates higher errors for a higher deficit of moisture (drier air) at ROTH. At TUCC, high correlations are found with the evaporation from impervious surfaces indicating this surface cover type might explain most of the errors. Overall, correlations are typically weaker at TUCC except for evaporation from impervious surfaces. We expect the weaker correlations to be a consequence of the lower MBE. In turn, the lower MBE may be partially explained by the lower range of observed ET as a consequence of the high impervious fraction.

Impervious surfaces contribute proportionally less to ET than their surface fraction according to the bottom-up approach (Figure 6a). In contrast, high vegetation contributes significantly more. The relative ET contribution of low vegetation varies depending on the composition of the remaining surfaces. In areas with mainly impervious surfaces, low vegetation exhibits a comparatively larger ET contribution, while in regions mainly covered by high vegetation, its ET contribution is lower. Despite open water covering only a small fraction of the surface, the TUCC results indicate that the ET fraction can exceed the surface fraction. The relative contributions are constant throughout the months, although exact fraction values vary mostly around 0.02 with exceptions up to 0.13. Throughout the study period, the surface fraction has the same qualitative relation to ET contribution.

The top-down approach yields similar relative contributions to the surface cover and ET as the bottom-up approach (Figure 6b). However, the ET fractions are more similar to the surface fractions than the bottom-up approach indicates. Noteworthy, the negligible open water surface contributes 20% to ET at ROTH. This result seems unlikely given that nearly no water bodies are within the area of most footprints at ROTH. Thus, it exposes a potential weakness of the top-down approach related to the data instead of the physics-driven nature of this approach. On top of that, in only 44 timesteps the linear system of equations resulted in a solution for two reasons. First, the data availability limits this approach to 342 timesteps. Subsequently, 298 timesteps are excluded from the analysis as negative evaporation rates artificially enhanced the evaporation from the other surfaces. This artificial enhancement is an artifact of the linear system of equations (Eq. 5). Next to the ET fractions, the surface fractions differ slightly from the bottom-up approach because different timesteps are considered. Over the months, relative ET contributions differ due to the low reliability of monthly estimates caused by the low data availability (not shown). In some months, the relative ET contribution becomes negative, which we attribute to artificially-enhanced evaporation from the linear system. Unlike the bottom-up approach, no direct comparison with observations can be made, as

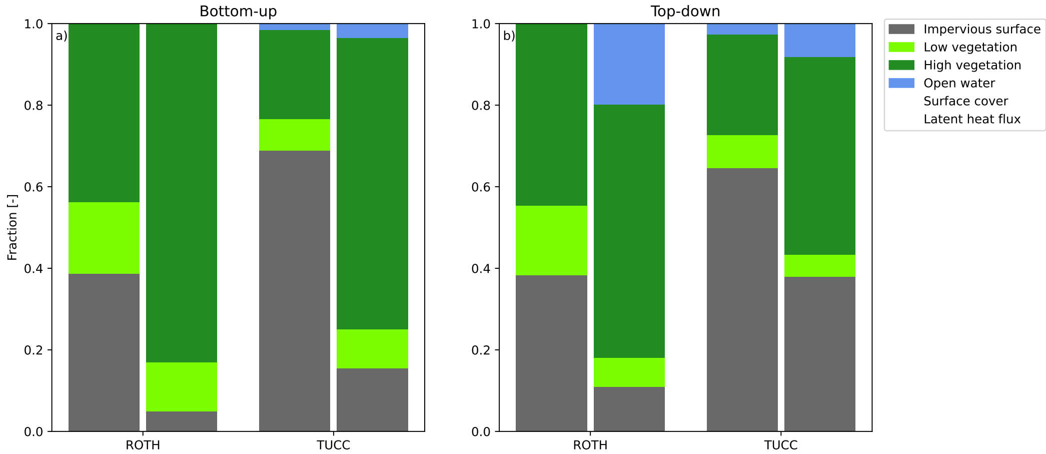

Figure 6. Relative contribution of the surface cover types to total surface cover (vertical/horizontal hatch) and ET (diagonal hatch). Surface cover fractions differ between the two methods at the same site at different times and thus footprints are included in the analysis due to data availability.

the method gets the EC observations as input, and no observations are available at the patch scale.

4.4 Evaporation dynamics per surface cover type

The distinct evaporation dynamics of each surface cover type are visible when zooming in on one drydown (Figure 7). These dynamics can be derived from the bottom-up approach given its good performance and the high number of timesteps with attributed fluxes. The impervious surface has a unique pattern with a sharp peak after rainfall and no evaporation once the surface has dried. Meanwhile, the other three surface cover types all show a daily cycle. Low vegetation and open water show comparable changes over time without a response to the time since the last precipitation but following energy availability and transport efficiency. On the other hand, high vegetation limits ET within days after rainfall. These responses are seen in all other dyrdowns except for the last drydown during the warm season. At this time, the soil moisture is more depleted triggering low vegetation to limit ET, while open water maintains the same response.

5 Discussion and conclusion

5.1 Surface cover type contributions to evapotranspiration

Our study revealed that the four distinguished surface cover types do not contribute to ET proportional to their surface fraction. To disentangle these contributions, the ET was attributed to the surface covers with both a bottom-up and top-down approach. Both approaches find similar ET contributions compared to the surface fraction; impervious surfaces evaporate less than their surface fraction, while high vegetation and open water evaporate more. For high vegetation, an isotope-evaluated model study found similar ratios between surface fraction ($\sim$30%) and ET contribution ($\sim$80%) at ROTH (Gillefalk et al., 2022). From this ET, evaporation of interception accounts for 17% of the total precipitation over the study period from April to October. This is comparable to some studies finding values between 14-27% (Bryant et al., 2005; Xiao & McPherson, 2011), while others show higher interception evaporation between 45 and 77% (Asadian & Weiler,

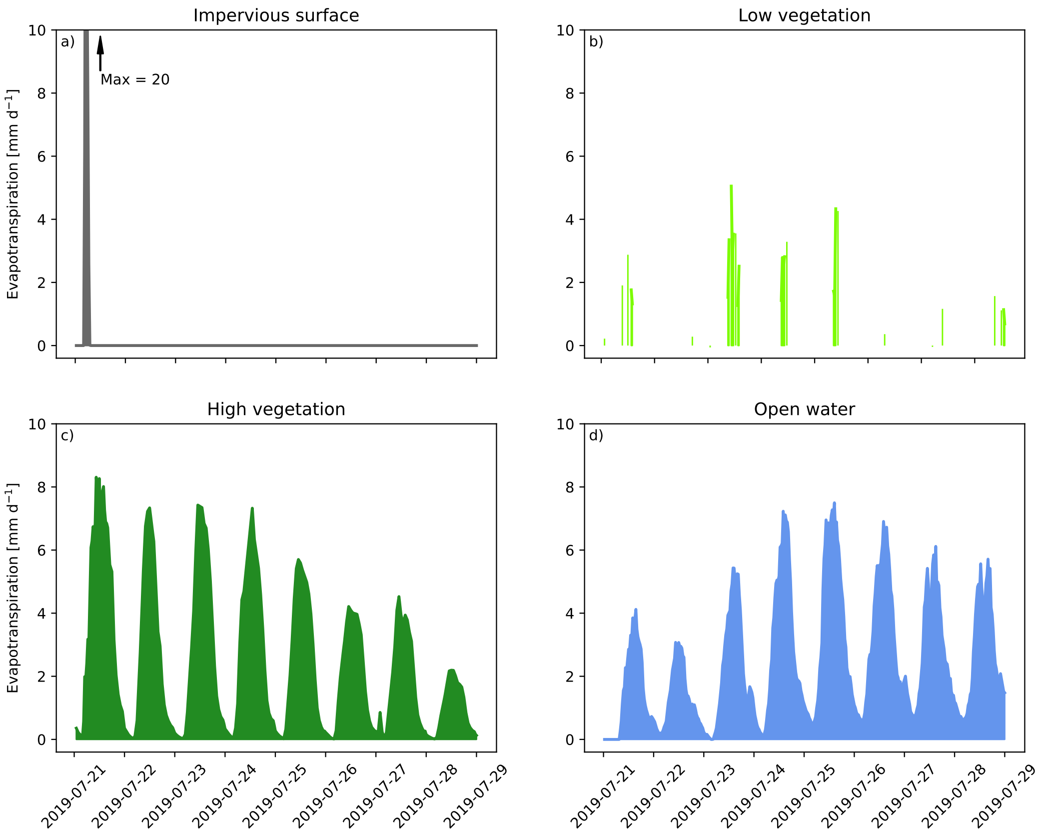

Figure 7. Illustration of *ET* dynamics during a drydown starting 30 minutes after rainfall ceased determined with the bottom-up approach for the four surface cover types (a: impervious surface, b: low vegetation, c: high vegetation, d: open water). This drydown occurred between 21-07-2019 and 29-07-2019. The gaps in the are explained by the quality control of the 2-m EC measuring low vegetation.

2009; Anys & Weiler, 2023) or lower between 5-6% (Paul-Limoges et al., 2020). Although our interception evaporation is lower than most observed values, together with transpiration, it exceeds the precipitation during the study period. Soil moisture reserves supply the additional water. For low vegetation, the ET contribution may either be higher or lower than their surface fraction depending on the composition of the other surfaces.

The found ET contributions are largely in line with findings by Peters et al. (2011), who did a similar exercise for a more homogeneous neighborhood. Still, we challenge their assumption that the impervious surface did not contribute anything to ET, as we find 5% (11% top-down) of ET may come from impervious surfaces in a suburban setting (ROTH, 39% impervious in footprint). In the more impervious city center (TUCC, 65/69% impervious in the footprint), we find a contribution of 15% (38% top-down). Ramamurthy and Bou-Zeid (2014); Chen et al. (2023) found ET from impervious surfaces contributed between 11 and 18%.

Even though the ET contribution was similar for the bottom-up and the top-down approach, these methodologies also showed two interesting differences. Given these two differences, we think the bottom-up approach has the most potential to contribute to our understanding of the link between patch- and neighborhood-scale ET. The first difference is the number of timesteps with a successful outcome: 1112 for bottom-up and 44 for top-down. The maximum number is limited by the study period of 244 days equal to 11,712 half hours for top-down, of which 2,196 are during the midday hours. The EC observations cause the high number of timesteps without results, as these EC observations contain considerable gaps, as many observations are filtered during quality control because of the challenging urban environment (Feigenwinter et al., 2012; Oke et al., 2017). Moreover, only the highest-quality EC observations are suitable for our analysis (quality flag "0" (Foken et al., 2004)), as this study focuses on the process level. While data availability is a challenge for both approaches, the top-down approach relies more heavily on EC observations leading to even fewer timesteps with results.

The second difference is that the bottom-up approach is driven by physics, while the top-down approach is based on mathematics. The physics-driven bottom-up approach provides insight into the ET contributions of the surface cover types but still has a mismatch with the observed ET. Also using a bottom-up approach, Salmond et al. (2012) reconstructed the neighborhood-scale sensible heat flux observed with an EC system with smaller-scale observations from two scintellometers. They found a mismatch of 25%, which can partly be explained by three reasons that also apply here. Firstly, even when EC systems are installed directly next to each other, the observations differ, up to 15% in the case of ET (Mauder et al., 2006, 2013). These differences are partly due to large turbulent structures that are not resolved at (sub-)hourly timescales. This makes time-averaged EC observations not by definition representative of the spatial average over heterogeneous surfaces. As these structures may resolve at daily timescales, it may explain the better performance of the bottom-up approach at the daily timescale. Secondly, the footprints are calculated with an analytical model that does not account for surface heterogeneity and 3-dimensional surfaces (more in Section 5.3). Lastly, the patch-scale observations are not necessarily representative of the whole neighborhood scale. In our case, for example, sap flow was measured at six trees that cannot capture the diversity of the trees in the EC footprint. Another example is the low vegetation that experiences shading depending on the location within the canyon.

Still, the physics-driven bottom-up approach yields errors comparable to urban land surface models from a decade ago and only slightly higher than more recent models (Grimmond et al., 2011; Lipson et al., 2023). Most urban land surface models assume the neighborhood flux is the sum of the separate surface covers. Compared to these models, our approach reduces complexity and requires fewer inputs. The found agreement underscores the potential for utilizing surface-specific contributions to decipher ET dynamics.

In contrast, the top-down approach yields highly unlikely results as the linear system follows mathematics instead of physics. The linear system counteracted high negative fluxes with high positive fluxes giving results as extreme as -2.0×10^{17} and 1.1×10^{6} mm d^{-1}. These effects were omitted from the analysis by excluding negative fluxes, which omitted the high fluxes as well due to the linear relations in the equations. Due to these direct links, the ET contributions contain the errors from the EC observations. However, these random errors will cancel out against each other, as we only look at aggregated results from the top-down results.

While open water contributes little to the surface cover, we included this surface cover type in our analysis. It cannot be assigned to any of the other surface cover types and its inclusion improves the transferability of our methodology. In the top-down approach, the low open water fraction caused extremely high or low evaporation fluxes, as these could be compensated with relatively small changes in surface cover types with larger fractions. In an attempt to eliminate this compensation, we performed the top-down analysis with only three surface cover types and three EC systems leaving out the 2-m EC at ROTH. As this EC system had the most data gaps, the number of timesteps with results rose from 44 to 527. Logically, no contribution from water is inferred. The impervious contribution rises with 8% (ROTH) and 15% (TUCC) but is still lower than its surface fraction. The low vegetation contributes more to ET with an increase of 37% (ROTH) and 17% (TUCC). Consequently, its ET contribution is now higher instead of lower than its surface fraction. Only, high vegetation has a lower ET contribution dropping 22% (ROTH) and 24% (TUCC). These changes show mathematical top-down approach can give considerably different results by changing the input.

5.2 Evaporation dynamics per surface cover type

Apart from the different ET contributions compared to the surface fraction, evaporation evolves differently for each surface cover after rainfall. Impervious surfaces evaporate all water quickly after rainfall, as was also found by (Ramamurthy & Bou-Zeid, 2014). In contrast, open water sustains evaporation for a longer time. The open water evaporation shows a strong daily trend reaching zero during the night. Previous research shows the large heat capacity of water dampens the daily trend, which does not go down to zero (Jansen et al., 2023). In this study, the daily trend results from the Penman equation (Jansen & Teuling, 2020), which was applied given the unavailability of water temperatures. High and low vegetation show different behavior from each other with the high vegetation having a higher initial ET. While high vegetation decreases ET within days after the last precipitation, low vegetation sustains high ET rates until soil moisture availability is limiting. This soil moisture limitation only occurred towards the end of the summer, even though our study year 2019 was relatively dry. The same responses were found in other studies (Teuling et al., 2010; van Dijke et al., 2023). High vegetation has a stronger stomatal control that enables it to limit transpiration with sufficient available moisture, while low vegetation keeps transpiring until it lacks water.

5.3 Footprint variability and modeling

Given these differences in evaporation behavior between surface cover types, the surface composition in the footprint influences the EC observations. This changing footprint has to be accounted for to understand ET dynamics, as the footprint contribution of a particular surface cover may vary as much as 50%. Previously, the relevance of footprints for ET was illustrated by the improved performance when the footprint-weighed surface cover was supplied to machine learning models in addition to meteorological observations (Vulova et al., 2021, 2023). For other fluxes, such as CO_2, footprint modeling has also been shown to help understand flux dynamics (e.g. Velasco et al., 2009; Conte & Contini, 2019; Wu et al., 2022).

CO_2 sources including directly from humans have been identified and quantified by looking at the relation between the CO_2 flux and the surface cover composition equivalent to Figure 4. For example, Stagakis et al. (2019) find that traffic is an important CO_2 source and human respiration accounts for 19% of the CO_2 flux. Human respiration and perspiration are unlikely to affect our results. In the center of Beijing, the water fluxes from these processes are so small they would account for only 3% of ET in Berlin (Liu et al., 2022). Given the lower population density of our sites, human respiration and perspiration are even lower. Thus, these small water fluxes from these sources are much smaller than ET and do not influence the results.

Footprint modeling is the key that connects the surface to the ET in this study. The key is however limited by the simplifications of the footprint model. Here, we applied the analytical model by Kljun et al. (2015), which generates perfectly symmetrical footprints. The model does not account for the complexity and heterogeneity of the urban morphology. More detailed footprint modeling would provide footprints depending on urban morphology, but this would also require more computational resources and thus limit the length of the period that can be studied.

5.4 Generalizability

Here, we studied ET in one city during the warm months of a single year, 2019, which was a relatively dry year in Berlin. While the climate and year-to-year variability may affect some aspects of the ET dynamics, others are likely to be more constant. The main aspect we expect to be relatively constant is the evolution of ET over a drydown. The impervious surface will evaporate with a short intense peak, open water will evaporate more constantly, and vegetation will respond to soil moisture. These general patterns may be the same, but the dynamics are altered by site characteristics such as plant species, building materials, and water depth. Still, we anticipate this effect to be smaller than the differences found between the four surface covers. Apart from site characteristics, weather conditions control how much each of the surface covers contributes to the ET (Jansen et al., 2023). The weather conditions determine the water availability (number and length of drydowns), energy availability (radiation and temperature), and exchange efficiency (wind and vapor pressure deficit). These conditions will lead to changed ET dynamics dependent on the season, the climate, and the year-to-year variability.

The unique 2019 dataset from Berlin allowed us to reconstruct the ET signal from EC systems. Although relatively common observations are required for the conceptual models of the open water and impervious surfaces, the data needed to estimate the evaporation dynamics of both vegetated surfaces is more specialized. These observations included low-level EC observations, tree sap flow, and multiple, continuous soil moisture sensors. In most cities, this will not be available. Instead, the vegetated surfaces could be modeled with the Penman-Monteith equation (Monteith, 1965). Grimmond and Oke (1991) have adapted this equation to urban environments and included the effect of water limitation. As a preliminary analysis, the Penman-Monteith equation was used to represent vegetation in the bottom-up approach. This analysis showed that despite an overestimation of ET, ET may be reconstructed with less specialized observations.

6 Conclusion

This study explores the link of neighborhood-scale ET to the surface cover at two sites in Berlin to estimate the contribution of each surface cover type to ET. This link is made starting from the ET dynamic from the surface cover types reconstructing the neighborhood-scale flux (bottom-up) and from four neighborhood-scale fluxes partitioned over the surface cover types through a linear system of equations (top-down). We find most ET originates from vegetation with especially high vegetation evaporating disproportionately more than its surface fraction. Even though impervious surfaces contribute less to ET on long timescales they evaporate substantially after rainfall. Therefore, they should not be ignored in urban water management. While both approaches support these conclusions, the bottom-up approach proved to be more successful than the top-down approach in linking the surface covers at the patch scale to the observations at the neighborhood scale.

We stress the importance of time-dependent EC footprints to understand ET dynamics. Based on these dynamics, urban land surface models and their evaluation could be improved by accounting for the changing footprint. With footprint information, parameters could be dependent on the situation in the current source area. In this way, the models would more directly represent what the EC system observes making for a more fair and better evaluation.

Understanding ET is crucial in urban water management, for example, to determine appropriate vegetation species and irrigation requirements. At the same time, ET plays a role in the energy balance and can contribute to the mitigation of heat stress. Therefore, the gained insights can support design decisions in city landscapes and urban water management to improve the living environment of urban inhabitants.

7 Open research

Spatial datasets are available at the Berlin Digital Environmental Atlas (Senate Department for Urban Development, Building and Housing, 2012, 2013; Senate Department for the Environment, Mobility, Consumer and Climate Protection Berlin, 2014). Rainfall observations can be accessed at the DWD Climate Data Center (DWD, 2021a). Sap flow and soil moisture data are available at the FRED open-access database of IGB (Kuhlemann et al., 2020). All other data in this publication is available at 4TU (citation at publication).

Acknowledgments

Special thanks to Judith Boekee, Studio Scientist, for the design of the conceptual figure, her tireless support, and her eye for detail. Harro Jongen acknowledges this research was supported by the WIMEK PhD grant 2020. Stenka Vulova was supported by the German Research Foundation (DFG) within the Research Training Group 'Urban Water Interfaces' (GRK 2032-2). Fred Meier acknowledges funding for instrumentation of the Urban Climate Observatory (UCO) Berlin from DFG grants SCHE 750/8 and SCHE 750/9 within Research Unit 1736 "Urban Climate and Heat Stress in Mid Latitude Cities in View of Climate Change (UCaHS)" and the research program "Urban Climate Under Change ([UC]2)", funded by the German Ministry of Research and Education (FKZ 01LP1602A).

References

Amt für Statistik Berlin-Brandenburg. (2019). *Das statistische informationssystem berlin-brandenburg.* Retrieved from `https://statis.statistik-berlin-brandenburg.de/webapi/jsf/tableView/tableView.xhtml` (Date accessed: 9 september 2021)

Anys, M., & Weiler, M. (2023). Rainfall interception of urban trees: event characteristics and tree morphological traits. *Preprint*.

Asadian, Y., & Weiler, M. (2009). A new approach in measuring rainfall interception by urban trees in coastal british columbia. *Water Quality Research Journal*, *44*(1), 16–25.

Aston, A. (1979). Rainfall interception by eight small trees. *Journal of hydrology*, *42*(3-4), 383–396.

Auvinen, M., Järvi, L., Hellsten, A., Rannik, Ü., & Vesala, T. (2017). Numerical framework for the computation of urban flux footprints employing large-eddy simulation and lagrangian stochastic modeling. *Geoscientific Model Development*, *10*(11), 4187–4205.

Baptista, M. D., Livesley, S. J., Parmehr, E. G., Neave, M., & Amati, M. (2018). Variation in leaf area density drives the rainfall storage capacity of individual urban tree species. *Hydrological processes*, *32*(25), 3729–3740.

Boese, S., Jung, M., Carvalhais, N., Teuling, A. J., & Reichstein, M. (2019). Carbon–water flux coupling under progressive drought. *Biogeosciences*, *16*(13), 2557–2572.

Bonneau, J., Fletcher, T. D., Costelloe, J. F., Poelsma, P. J., James, R. B., & Burns, M. J. (2018). Where does infiltrated stormwater go? interactions with vegetation and subsurface anthropogenic features. *Journal of Hydrology*, *567*, 121–132.

Bryant, M. L., Bhat, S., & Jacobs, J. M. (2005). Measurements and modeling of throughfall variability for five forest communities in the southeastern us. *Journal of Hydrology*, *312*(1-4), 95–108.

Chen, H., Huang, J. J., Liang, H., Wang, W., Li, H., Wei, Y., ... Zhang, P. (2023). Can evaporation from urban impervious surfaces be ignored? *Journal of Hydrology*, *616*, 128582.

Conte, M., & Contini, D. (2019). Size-resolved particle emission factors of vehicular traffic derived from urban eddy covariance measurements. *Environmental Pollution*, *251*, 830–838.

De Bruin, H. (1979). Neerslag, openwaterverdamping en potentieel neerslagoverschot in nederland, frequentieverdelingen in het groeiseizoen. *WR 79-04*.

Duarte Rocha, A., Vulova, S., van der Tol, C., Förster, M., & Kleinschmit, B. (2022). Modelling hourly evapotranspiration in urban environments with scope using open remote sensing and meteorological data. *Hydrology and earth system sciences*, *26*(4), 1111–1129.

DWD. (2021a). *Dwd climate data center (cdc).* Retrieved from `https://opendata.dwd.de/climate_environment/CDC/observations_germany/climate/` (Date accessed: 9 september 2021)

DWD. (2021b). *Vieljährige mittelwerte.* Retrieved from `https://www.dwd.de/DE/leistungen/klimadatendeutschland/vielj_mittelwerte.html` (Date accessed: 9 september 2021)

Feigenwinter, C., Vogt, R., & Christen, A. (2012). Eddy covariance measurements over urban areas. *Eddy covariance: A practical guide to measurement and data analysis*, 377–397.

Fenner, D., Christen, A., Chrysoulakis, N., Grimmond, S., Van Hove, M., Kotthaus, S., ... Zeeman, M. (2023). *Impact of a large isolated city on the mixed layer height during different weather conditions* (Tech. Rep.). Copernicus Meetings.

Fenner, D., Meier, F., Scherer, D., & Polze, A. (2014). Spatial and temporal air temperature variability in berlin, germany, during the years 2001–2010. *Urban Climate*, *10*, 308–331.

Fletcher, T. D., Andrieu, H., & Hamel, P. (2013). Understanding, management and modelling of urban hydrology and its consequences for receiving waters: A state of the art. *Advances in water resources*, *51*, 261–279.

Foken, T., Göockede, M., Mauder, M., Mahrt, L., Amiro, B., & Munger, W. (2004). Post-field data quality control. In *Handbook of micrometeorology: a guide for surface flux measurement and analysis* (pp. 181–208). Springer.

Gillefalk, M., Tetzlaff, D., Hinkelmann, R., Kuhlemann, L.-M., Smith, A., Meier, F., ... Soulsby, C. (2021). Quantifying the effects of urban green space on water partitioning and ages using an isotope-based ecohydrological model. *Hydrology and Earth System Sciences*, *25*(6), 3635–3652.

Gillefalk, M., Tetzlaff, D., Marx, C., Smith, A., Meier, F., Hinkelmann, R., &

Soulsby, C. (2022). Estimates of water partitioning in complex urban landscapes with isotope-aided ecohydrological modelling. *Hydrological Processes*, *36*(3), e14532.

Grimmond, C. S. B., Blackett, M., Best, M. J., Baik, J.-J., Belcher, S., Beringer, J., ... others (2011). Initial results from phase 2 of the international urban energy balance model comparison. *International Journal of Climatology*, *31*(2), 244–272.

Grimmond, C. S. B., & Oke, T. R. (1991). An evapotranspiration-interception model for urban areas. *Water resources research*, *27*(7), 1739–1755.

Gunawardena, K. R., Wells, M. J., & Kershaw, T. (2017). Utilising green and bluespace to mitigate urban heat island intensity. *Science of the Total Environment*, *584*, 1040–1055.

Haacke, N. (2022). *Scaling and connectivity assessment of critical source areas of diffuse pollution in urban catchments under a changing regime of high-intensity storms* (PhD thesis). Technischen Universität Berlin. (https://doi.org/10.14279/depositonce-16434)

Heaviside, C., Macintyre, H., & Vardoulakis, S. (2017). The urban heat island: implications for health in a changing environment. *Current environmental health reports*, *4*, 296–305.

Hellsten, A., Luukkonen, S.-M., Steinfeld, G., Kanani-Sühring, F., Markkanen, T., Järvi, L., ... Raasch, S. (2015). Footprint evaluation for flux and concentration measurements for an urban-like canopy with coupled lagrangian stochastic and large-eddy simulation models. *Boundary-Layer Meteorology*, *157*, 191–217.

Herwitz, S. R. (1985). Interception storage capacities of tropical rainforest canopy trees. *Journal of Hydrology*, *77*(1-4), 237–252.

Hsieh, C.-I., Siqueira, M., Katul, G., & Chu, C.-R. (2003). Predicting scalar source-sink and flux distributions within a forest canopy using a 2-d lagrangian stochastic dispersion model. *Boundary-layer meteorology*, *109*, 113–138.

Huang, J. Y., Black, T., Jassal, R., & Lavkulich, L. L. (2017). Modelling rainfall interception by urban trees. *Canadian Water Resources Journal/Revue Canadienne des Ressources Hydriques*, *42*(4), 336–348.

Jacobs, C., Klok, L., Bruse, M., Cortesão, J., Lenzholzer, S., & Kluck, J. (2020). Are urban water bodies really cooling? *Urban Climate*, *32*, 100607.

Jansen, F. A., Jongen, H. J., Jacobs, C. M., Bosveld, F. C., Buzacott, A. J., Heusinkveld, B. G., ... others (2023). Land cover control on the drivers of evaporation and sensible heat fluxes: An observation-based synthesis for the netherlands. *Water Resources Research*, *59*(11), e2022WR034361.

Jansen, F. A., & Teuling, A. J. (2020). Evaporation from a large lowland reservoir–(dis) agreement between evaporation models from hourly to decadal timescales. *Hydrology and Earth System Sciences*, *24*(3), 1055–1072.

Jansen, F. A., Uijlenhoet, R., Jacobs, C. M., & Teuling, A. J. (2022). Evaporation from a large lowland reservoir–observed dynamics and drivers during a warm summer. *Hydrology and Earth System Sciences*, *26*(11), 2875–2898.

Jin, L., Schubert, S., Fenner, D., Meier, F., & Schneider, C. (2021). Integration of a building energy model in an urban climate model and its application. *Boundary-Layer Meteorology*, *178*(2), 249–281.

Jongen, H. J., Steeneveld, G.-J., Beringer, J., Christen, A., Chrysoulakis, N., Fortuniak, K., ... others (2022). Urban water storage capacity inferred from observed evapotranspiration recession. *Geophysical Research Letters*, *49*(3), e2021GL096069.

Karl, T., Lamprecht, C., Graus, M., Cede, A., Tiefengraber, M., Vila-Guerau de Arellano, J., ... Lenschow, D. (2023). High urban no x triggers a substantial chemical downward flux of ozone. *Science Advances*, *9*(3), eadd2365.

Klaassen, W., Bosveld, F., & De Water, E. (1998). Water storage and evaporation as constituents of rainfall interception. *Journal of Hydrology*, *212*, 36–50.

Kljun, N., Calanca, P., Rotach, M., & Schmid, H. P. (2015). A simple two-dimensional parameterisation for flux footprint prediction (ffp). *Geoscientific Model Development*, *8*(11), 3695–3713.

Kljun, N., Rotach, M., & Schmid, H. (2002). A three-dimensional backward lagrangian footprint model for a wide range of boundary-layer stratifications. *Boundary-Layer Meteorology*, *103*, 205–226.

Kormann, R., & Meixner, F. X. (2001). An analytical footprint model for non-neutral stratification. *Boundary-Layer Meteorology*, *99*, 207–224.

Kottek, M., Grieser, J., Beck, C., Rudolf, B., & Rubel, F. (2006). *World map of the köppen-geiger climate classification updated.*

Kuhlemann, L.-M., Tetzlaff, D., Smith, A., Kleinschmit, B., & Soulsby, C. (2020). *Soil moisture data for grassland, shrub and trees at the steglitz urban ecohydrological observatory [data set].* IGB Leibniz-Institute of Freshwater Ecology and Inland Fisheries. doi: https://doi.org/10.18728/566.0

Kuhlemann, L.-M., Tetzlaff, D., Smith, A., Kleinschmit, B., & Soulsby, C. (2021). Using soil water isotopes to infer the influence of contrasting urban green space on ecohydrological partitioning. *Hydrology and Earth System Sciences*, *25*(2), 927–943.

Leclerc, M. Y., Shen, S., & Lamb, B. (1997). Observations and large-eddy simulation modeling of footprints in the lower convective boundary layer. *Journal of Geophysical Research: Atmospheres*, *102*(D8), 9323–9334.

Lipson, M. J., Grimmond, C. S. B., Best, M., Abramowitz, G., Coutts, A., Tapper, N., … Pitman, A. J. (2023). Evaluation of 30 urban land surface models in the urban-plumber project: Phase 1 results. *Quarterly journal of the Royal Meteorological Society*.

Lipson, M. J., Grimmond, S., Best, M., Chow, W. T., Christen, A., Chrysoulakis, N., … others (2022). Harmonized gap-filled datasets from 20 urban flux tower sites. *Earth system science data*, *14*(11), 5157–5178.

Liu, C., Liu, J., Shao, W., Lu, J., & Gao, H. (2022). The considerable water evaporation induced by human perspiration and respiration in megacities: Quantifying method and case study in beijing. *International Journal of Environmental Research and Public Health*, *19*(14), 8638.

Mauder, M., Cuntz, M., Drüe, C., Graf, A., Rebmann, C., Schmid, H. P., … Steinbrecher, R. (2013). A strategy for quality and uncertainty assessment of long-term eddy-covariance measurements. *Agricultural and Forest Meteorology*, *169*, 122–135.

Mauder, M., Liebethal, C., Göckede, M., Leps, J.-P., Beyrich, F., & Foken, T. (2006). Processing and quality control of flux data during litfass-2003. *Boundary-Layer Meteorology*, *121*, 67–88.

McGrane, S. J. (2016). Impacts of urbanisation on hydrological and water quality dynamics, and urban water management: a review. *Hydrological Sciences Journal*, *61*(13), 2295–2311.

Meier, F., & Scherer, D. (2012). Spatial and temporal variability of urban tree canopy temperature during summer 2010 in berlin, germany. *Theoretical and Applied Climatology*, *110*, 373–384.

Monteith, J. L. (1965). Evaporation and environment. In *Symposia of the society for experimental biology* (Vol. 19, pp. 205–234).

Nicolini, G., Antoniella, G., Carotenuto, F., Christen, A., Ciais, P., Feigenwinter, C., … others (2022). Direct observations of co2 emission reductions due to covid-19 lockdown across european urban districts. *Science of the Total Environment*, *830*, 154662.

Oke, T. R. (1982). The energetic basis of the urban heat island. *Quarterly journal of the royal meteorological society*, *108*(455), 1–24.

Oke, T. R., Mills, G., Christen, A., & Voogt, J. A. (2017). *Urban climates.* Cambridge University Press.

Paul, M., & Meyer, J. (2001). Streams in the urban landscape. *Annual Review of Ecology and Systematics*, *32*, 333-365.

Paul-Limoges, E., Wolf, S., Schneider, F. D., Longo, M., Moorcroft, P., Gharun, M., & Damm, A. (2020). Partitioning evapotranspiration with concurrent eddy covariance measurements in a mixed forest. *Agricultural and Forest Meteorology*, *280*, 107786.

Penman, H. (1956). Evaporation: an introductory survey. *Netherlands Journal of Agricultural Science*, *4*(1), 9–29.

Peters, E. B., Hiller, R. V., & McFadden, J. P. (2011). Seasonal contributions of vegetation types to suburban evapotranspiration. *Journal of Geophysical Research: Biogeosciences*, *116*(G1).

Qin, L., Yan, C., Yu, L., Chai, M., Wang, B., Hayat, M., ... others (2022). High-resolution spatio-temporal characteristics of urban evapotranspiration measured by unmanned aerial vehicle and infrared remote sensing. *Building and Environment*, *222*, 109389.

Ramamurthy, P., & Bou-Zeid, E. (2014). Contribution of impervious surfaces to urban evaporation. *Water Resources Research*, *50*(4), 2889–2902.

Ramírez, B. H., Melsen, L. A., Ganzeveld, L., Leemans, R., & Teuling, A. J. (2018). Tropical montane cloud forests in the orinoco river basin: Inferring fog interception from through-fall dynamics. *Agricultural and Forest Meteorology*, *260*, 17–30.

Rocha, A. D., Vulova, S., Meier, F., Förster, M., & Kleinschmit, B. (2022). Mapping evapotranspirative and radiative cooling services in an urban environment. *Sustainable Cities and Society*, *85*, 104051. doi: 10.1016/j.scs.2022.104051

Rutter, A., Morton, A., & Robins, P. (1975). A predictive model of rainfall interception in forests. ii. generalization of the model and comparison with observations in some coniferous and hardwood stands. *Journal of Applied Ecology*, 367–380.

Salmond, J., Roth, M., Oke, T., Christen, A., & Voogt, J. (2012). Can surface-cover tiles be summed to give neighborhood fluxes in cities? *Journal of applied meteorology and climatology*, *51*(1), 133–149.

Scherer, D., Ament, F., Emeis, S., Fehrenbach, U., Leitl, B., Scherber, K., ... Vogt, U. (2019). Three-dimensional observation of atmospheric processes in cities. *Meteorol Z*, *28*(2), 121–138.

Schmid, H., & Oke, T. (1990). A model to estimate the source area contributing to turbulent exchange in the surface layer over patchy terrain. *Quarterly Journal of the Royal Meteorological Society*, *116*(494), 965–988.

Schuepp, P., Leclerc, M., MacPherson, J., & Desjardins, R. (1990). Footprint prediction of scalar fluxes from analytical solutions of the diffusion equation. *Boundary-Layer Meteorology*, *50*(1-4), 355–373.

Senate Department for the Environment, Mobility, Consumer and Climate Protection Berlin. (2014). *Straßenbefahrung 2014 - [wms].* Retrieved from `https://daten.berlin.de/datensaetze/stra%C3%9Fenbefahrung-2014-wms` (Date accessed: 21 September 2023)

Senate Department for Urban Development, Building and Housing. (2012). *Building and vegetation heights 2012.* Retrieved from `https://www.berlin.de/umweltatlas/en/land-use/building-heights/2012/summary/` (Date accessed: 21 September 2023)

Senate Department for Urban Development, Building and Housing. (2013). *Biotope types 2013.* Retrieved from `https://www.berlin.de/umweltatlas/en/biotopes/biotope-types/continually-updated/summary/` (Date accessed: 21 September 2023)

Solcerova, A., Van de Ven, F., & Van de Giesen, N. (2019). Nighttime cooling of an urban pond. *Frontiers in earth science*, *7*, 156.

Stagakis, S., Chrysoulakis, N., Spyridakis, N., Feigenwinter, C., & Vogt, R. (2019). Eddy covariance measurements and source partitioning of co2 emissions in an urban environment: Application for heraklion, greece. *Atmospheric Environment*, *201*, 278–292.

Steeneveld, G. J., Koopmans, S., Heusinkveld, B. G., & Theeuwes, N. E. (2014). Refreshing the role of open water surfaces on mitigating the maximum urban heat island effect. *Landscape and Urban Planning*, *121*, 92–96.

Teuling, A. J., Seneviratne, S. I., Stöckli, R., Reichstein, M., Moors, E., Ciais, P., ... others (2010). Contrasting response of european forest and grassland energy exchange to heatwaves. *Nature geoscience*, *3*(10), 722–727.

Teuling, A. J., Seneviratne, S. I., Williams, C., & Troch, P. (2006). Observed timescales of evapotranspiration response to soil moisture. *Geophysical Research Letters*, *33*(23).

Theeuwes, N. E., Solcerova, A., & Steeneveld, G. J. (2013). Modeling the influence of open water surfaces on the summertime temperature and thermal comfort in the city. *Journal of Geophysical Research: Atmospheres*, *118*(16), 8881–8896.

Valente, F., David, J., & Gash, J. (1997). Modelling interception loss for two sparse eucalypt and pine forests in central portugal using reformulated rutter and gash analytical models. *Journal of hydrology*, *190*(1-2), 141–162.

van Dijke, A. J. H., Orth, R., Teuling, A. J., Herold, M., Schlerf, M., Migliavacca, M., ... Mallick, K. (2023). Comparing forest and grassland drought responses inferred from eddy covariance and earth observation. *Agricultural and Forest Meteorology*, *341*, 109635.

Velasco, E., Pressley, S., Grivicke, R., Allwine, E., Coons, T., Foster, W., ... others (2009). Eddy covariance flux measurements of pollutant gases in urban mexico city. *Atmospheric Chemistry and Physics*, *9*(19), 7325–7342.

Vesala, T., Kljun, N., Rannik, Ü., Rinne, J., Sogachev, A., Markkanen, T., ... Leclerc, M. Y. (2008). Flux and concentration footprint modelling: State of the art. *Environmental Pollution*, *152*(3), 653–666.

Vulova, S., Kuhlemann, L.-M., Tetzlaff, D., Soulsby, C., & Kleinschmit, B. (2019). Assessment of evapotranspiration from urban vegetation across space and time: a case study in berlin. In *2019 10th international workshop on the analysis of multitemporal remote sensing images (multitemp)* (pp. 1–4).

Vulova, S., Meier, F., Rocha, A. D., Quanz, J., Nouri, H., & Kleinschmit, B. (2021). Modeling urban evapotranspiration using remote sensing, flux footprints, and artificial intelligence. *Science of The Total Environment*, *786*, 147293.

Vulova, S., Rocha, A. D., Meier, F., Nouri, H., Schulz, C., Soulsby, C., ... Kleinschmit, B. (2023). City-wide, high-resolution mapping of evapotranspiration to guide climate-resilient planning. *Remote Sensing of Environment*, *287*, 113487.

Wang, W., & Davis, K. J. (2008). A numerical study of the influence of a clearcut on eddy-covariance fluxes of co2 measured above a forest. *agricultural and forest meteorology*, *148*(10), 1488–1500.

Wang, W., & Shu, J. (2020). Urban renewal can mitigate urban heat islands. *Geophysical Research Letters*, *47*(6), e2019GL085948.

Ward, H., & Grimmond, C. (2017). Assessing the impact of changes in surface cover, human behaviour and climate on energy partitioning across greater london. *Landscape and Urban Planning*, *165*, 142–161.

Wouters, H., Demuzere, M., De Ridder, K., & van Lipzig, N. P. (2015). The impact of impervious water-storage parametrization on urban climate modelling. *Urban Climate*, *11*, 24–50.

Wu, K., Davis, K. J., Miles, N. L., Richardson, S. J., Lauvaux, T., Sarmiento, D. P., ... others (2022). Source decomposition of eddy-covariance co2 flux measurements for evaluating a high-resolution urban co2 emissions inventory. *Environmental Research Letters*, *17*(7), 074035.

Xiao, Q., & McPherson, E. G. (2011). Rainfall interception of three trees in oakland, california. *Urban Ecosystems*, *14*, 755–769.

Zeeman, M., Benjamins, K., Briegel, F., Drouin, M.-A., Feigel, G., Fenner, D., ... others (2023). *A modular data management approach for environmental observation campaigns in multiple cities* (Tech. Rep.). Copernicus Meetings.

Zimmermann, F., Köstler, H., Grabowski, C., Moeck, M., Saure, C., & Kielhorn, K.-H. (2015, May). *Beschreibung der biotoptypen.*